NUMERICAL INVESTIGATION OF FLOW OVER SHRAPNEL / SHELL DISCARDING CONFIGURATION

Liu Sen
Aircraft Engineering Department , Northwestern Polytechnical University
Xi'an, Shaanxi, 710072, P.R.China

Abstract

As a new attempt to numerically study the complex multibody aerodynamics , Euler equations are solved in this paper , with the employment of a kind of explict TVD scheme and the Overlapped Grid technique , to investigate the interfered supersonic flow field about a shrapnel / shell discarding configuration . Computational results have shown the existance of strong aerodynamic interference among shrapnel corebody and the discarded shells, which causes their aerodynamic characteristics to differ from that without any interference .

Introduction

With the development of aerospace technology , more and more multibody flight vehicles have emerged , e.g. the carrier airplane mounted by a large structure such as the shuttle orbiter freighted by a Boeing-747, and the rocket with strap-on boosters. It is necessary to investigate the aerodynamic interference among these bodies . If there is multibody separation just like the booster / orbiter separation , we must study the factors affecting separation safety conditions as well .

The shrapnel / shell discarding discussed here is a typical multibody interference , multibody separation problem (as sketched in Fig. 1). At the early stage of shell discarding , one corebody and four pieces of shells co-exist in the vicinity of each other , and we are deeply concerned about whether corebody and shells will collide . However , it has always been difficult to study multibody interference and separation because of the complexity of interfered flow and the unsteadiness of separation process . With regard to the problem of corebody / shell discarding , most of the previous works are experimental research [1,2]and the merely few theoretical and numerical works are engineering approximaions which can not reveal the complicated wave reflection and intersection[3,4]. The only numerical work was done by Nusca in 1990 , who solved the NS equations for simplified projectile / sabot discarding problem [5].

The two key points of multibody computational aerodynamics are : (1)generation of computational grids fitting all of the body surfaces , and (2)construction of proper scheme dealing with the complex flow struc ture.

The whole flow field in this paper is divided into two parts , namely the non-interfered Region Ⅰ and the interfered Region Ⅱ as shown in Fig 2 .

In Region Ⅰ , unsteady axisymmetric Euler equations are solved with a time marching method to provide initial data for Region Ⅱ , where 3-D steady Euler equations are solved by space marching from the initial data plane .

According to the two key points mentioned above , the Overlapped Grid method is adopted to generate all-surface-fitting grid in Region Ⅱ , together with the NND scheme (Non-oscillation , non-free-parameter, Dissipative scheme , virtully a kind of TVD scheme proposed by Prof. Zhang H.X. of CARDC[6]) .

Computation in Region Ⅰ

The computational mothod here is the ordinary splitting coefficient matrics(SCM) approch described in detail in Ref. 7 and briefly reviewed here .

The governing equations are in non-conservative form :

$$\vec{d}_t + A\vec{d}_x + B\vec{d}_y + C\vec{d}_z + \vec{c} = 0 \tag{1}$$

Splitting the coefficient matrices , we get

$$\vec{d}_t + A_+\vec{dx}_b + A_-\vec{dx}_f + B_+\vec{dy}_b + B_-\vec{dy}_f + C_+\vec{dz}_b + C_-\vec{dz}_f + \vec{c} = 0 \tag{2}$$

where all of the variables are defined in Ref.7 .

The characteristic relation is used at solid wall , and the main shock wave is fitted . Solution is marched in time to get the steady flow field in front of the shoulder plane of corebody.

Computation in Region Ⅱ

Because of the symmetry of flow , each space marching plane , which is perpendicular to corebody axis , is divided into 8 fan-like sections, and the space marching is performed in one of these sections, as shown in Fig.3

Governing Equations

3–D steady conservative Euler equations in curvilinear coordinates are

$$\frac{\partial \mathbf{E}}{\partial \xi}+\frac{\partial \mathbf{F}}{\partial \eta}+\frac{\partial \mathbf{G}}{\partial \zeta}=0 \tag{3}$$

where

$$\mathbf{E}=(\xi_x\cdot\mathbf{E}_1+\xi_y\cdot\mathbf{F}_1+\xi_z\cdot\mathbf{G}_1)/J$$
$$\mathbf{F}=(\eta_x\cdot\mathbf{E}_1+\eta_y\cdot\mathbf{F}_1+\eta_z\cdot\mathbf{G}_1)/J$$
$$\mathbf{G}=(\zeta_x\cdot\mathbf{E}_1+\zeta_y\cdot\mathbf{F}_1+\zeta_z\cdot\mathbf{G}_1)/J$$
$$J=\frac{\partial(\xi,\eta,\zeta)}{\partial(x,y,z)}$$
$$\mathbf{E}_1=(\rho u,\rho u^2+p,\rho uv,\rho uw,u(e+p))^T$$
$$\mathbf{F}_1=(\rho v,\rho uv,\rho v^2+p,\rho vw,v(e+p))^T$$
$$\mathbf{G}_1=(\rho w,\rho uw,\rho vw,\rho w^2+p,w(e+p))^T$$

ξ, η, ζ are axis , radius and circumference directions respectively .

Discretization and Stability

Eq(3) is discretized as follow :

in ξ direction , namely space marching direction , the predictor–corrector method is used to ensure 2nd order accuracy :

$$\overline{\mathbf{E}^{n+1}}=\mathbf{E}^n-\triangle\xi(\mathbf{F}_\eta+\mathbf{G}_\zeta)^n$$
$$\overline{\overline{\mathbf{E}^{n+1}}}=\mathbf{E}^{\overline{n+1}}-\triangle\xi(\mathbf{F}_\eta+\mathbf{G}_\zeta)^{\overline{n+1}} \tag{4}$$
$$\mathbf{E}^{n+1}=(\mathbf{E}^n+\overline{\overline{\mathbf{E}^{n+1}}})/2$$

where $\mathbf{F}_\eta$,$\mathbf{G}_\zeta$ are discretized with NND scheme :

$$\mathbf{F}_{\eta_j}=\frac{1}{\triangle\eta}(\widetilde{\mathbf{F}}_{j+\frac12}-\widetilde{\mathbf{F}}_{j-\frac12}) \tag{5}$$
$$\widetilde{\mathbf{F}}_{j+\frac12}=\mathbf{F}^+_{j+\frac12,L}+\mathbf{F}^-_{j+\frac12,R}$$
$$\mathbf{F}^+_{j+\frac12,L}=\mathbf{F}^+_j+\frac12\,\mathrm{minmod}\left(\triangle\mathbf{F}^+_{j-\frac12},\triangle\mathbf{F}^+_{j+\frac12}\right)$$
$$\mathbf{F}^-_{j+\frac12,R}=\mathbf{F}^-_{j+1}-\frac12\,\mathrm{minmod}\left(\triangle\mathbf{F}^-_{j+\frac12},\triangle\mathbf{F}^-_{j+\frac32}\right)$$

Limit function minmod(x,y) is

$$\mathrm{minmod}(x,y)=\begin{cases}0 & xy<0\\ x & |x|\leqslant|y|,\ xy>0\\ y & |x|>|y|,\ xy>0\end{cases}$$

and the discretization of $\mathbf{G}_\zeta$ is the same as $\mathbf{F}_\eta$

To perform a stable calculation , the dependent domain of difference equation must include that of differential equation . Based on characteristic analysis , the space marching step size must be limited as

$$\triangle\xi\leqslant C_N\cdot\min(A_2,A_3,B_2,B_3) \tag{6}$$

if $\xi=x$, then

$$A_2=\frac{\triangle\eta(u^2-a^2)}{\left|uV-\eta_x a^2\right|+a\sqrt{(V-u\eta_x)^2+(u^2-a^2)(\eta_y^2+\eta_z^2)}}$$

$$A_3=\frac{\triangle\zeta(u^2-a^2)}{\left|uW-\zeta_x a^2\right|+a\sqrt{(W-u\zeta_x)^2+(u^2-a^2)(\zeta_y^2+\zeta_z^2)}}$$
$$B_2=\triangle\eta\cdot u/V,\qquad B_3=\triangle\zeta\cdot u/W$$
$$V=\eta_x\cdot u+\eta_y\cdot v+\eta_z\cdot w$$
$$W=\zeta_x\cdot u+\zeta_y\cdot v+\zeta_z\cdot w$$

a is the sonic speed , and Courant number C_N should be less than 2 / 3 .

Computational Grids

For the configuration shown in Fig 1,2 and 3 , it is very difficult to generate a grid fitting corebody and shell surfaces at the same time , especially when they are closely located . So the Overlapped Grid is used in each space marching plane . A Core grid (called C grid) is generated only fit to corebody surface , while a Shell grid (called S grid) only fit to shell surface . These two grids have an overlapped region , as shown in Fig. 4 as region A′B′C′D′EFGHA′ , through which the grids exchange their flow field information . To some extent , we can regard this kind of information exchange as the interference between shells and corebody . The overlapped grids are shown in Fig. 5 .

Computational Sequence

After the completion of time marching in Region Ⅰ , flow parameters in the corebody shoulder plane is available , then the space marching in Region Ⅱ is started from the initial plane . S grid and C grid are generated when space marching reaches the leading edge of shell , and space marching is performed in these two grids individually , with the smaller marching step of the two grids as common marching step . At each step followed , the parameters on C grid boundary in overlapped region are interpolated from S grid , and vice versa .

Results and Disscusion

The free stream Mach number is $M_\infty=4.95$, and corebody angle of attack remains zero , while four pieces of shells are discarded symmetrically . The calculation , which is performed on VAX–Ⅱ micro–computer , provides us with an insight into the interference flow field .

In Fig.6 , the complexity of aerodynamic inteference is clearly shown . There exist reflection and intersection of shock wave and expansion wave . As the result of wave reflection , the pressure distribution along lower surface of

shells is in a wavy formation , as shown in fig.7 .

The 3–dimensionality of flow at the shell side edge is also clear , because the shell side edges are not enclosed . Fig.8–a shows the velocity vector in corebody shoulder plane (X = 0.0) , where there is no interference , and the flow is obviously axisymmetric . However , Fig. 8–b,c and d show the acceleration of flow at shell side edge from its lower surface to upper surface . The further the space marching goes ahead , the larger the region of 3–dimensionality becomes . Fig. 9–a,b,c and d are the iso–pressure contours corresponding to Fig. 8–a,b,c and d respectively .

Because of the wavy distribution of pressure , the aerodynamic forces acting on shells are much different from the freestream cases . Table 1 shows the variation of shell pressure center when shell is located at different places with different attitudes in the main bow shock layer . What should be noted is that , this movement of pressure center may cause the collision between shell and corebody .

Concluding Remarks

The calculation results have shown that , furious aerodynamic interference exists among shrapnel and shells , including reflection and intersection of shock wave and expansion wave . This interference results in unusual variation of aerodynamic forces , and the shell pressure center moves forward and backward when shell is at different places and attitudes in the main shock layer . This kind of effect may endanger shrapnel corebody and reduce its trajectory precision .

Additionally , the Overlapped Grid technique is capable of solving the problem of multibody–fitted grid generation , and the NND scheme behaves well in the computation of inviscid flow with complicated wave system .

Acknowledgement

The authors would like to thank Mr. Zhang L. M. Gao S.C. , Yie Y.D. , Yang Y.J. , Cheng Q.K. and Den X.G. for their helpful discussion and suggestion .

References

[1] E.M. Schmidt , " Wind Tunnel Meassurements of Sabot–Discarding Aerodynamics ", J. of Spacecraft and Rockets , Vol.18 , No.3 , pp235–245

[2] E.M. Schmidt , " Aerodynamic Interference during Sabot Discarding ", J. of Spacecraft and Rockets , Vol.15 , No.3 , pp162–167

[3] D. Siegelman, et al , " Projectile / Sabot Discard Aerodynamics ", AIAA Atmospheric Flight Mechanics Conference , 1980, pp280–286

[4] Lian J.C. , " Aerodynamics of Reentry Vehicle / Shell Discarding ", Technical Report of CARDC , 1982

[5] M. Nusca , " CFD Application to the Aerodynamics of Symmetric Sabot Discard ", AIAA 90–3096

[6] Zhang H.X. , " Non–oscillation , Non–free–parameter , Dissipative Differenc Scheme ", Proceedings of the 4th National CFD Conference , 1988

[7] Zhang L.M. , " Splitting Coefficient Matrics Method for the Solution to Hyperbolic System " , J. of Computational Physics , Vol.2 , No.3, pp269–274

[8] Liu Sen , " Aerodynamic Investigation of Reentry Shrapnel / Shell Discarding " , Thesis of Master Degree , Graduate School of CARDC , 1991

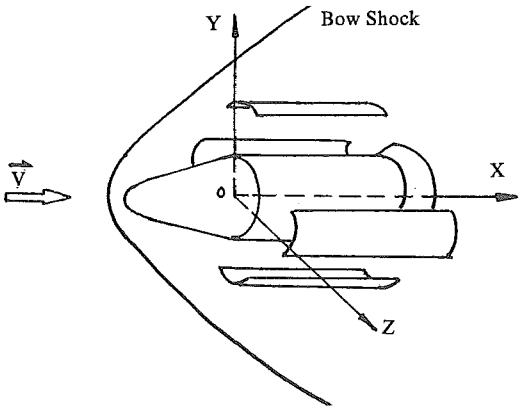

Figure 1 Reentry Shrapnel / Shell Discarding Configuration

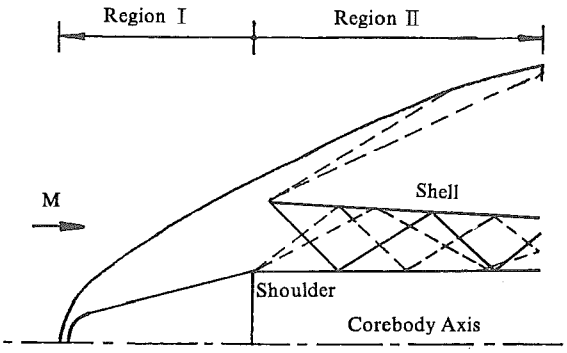

Figure 2 Two Regions of the Flow Field

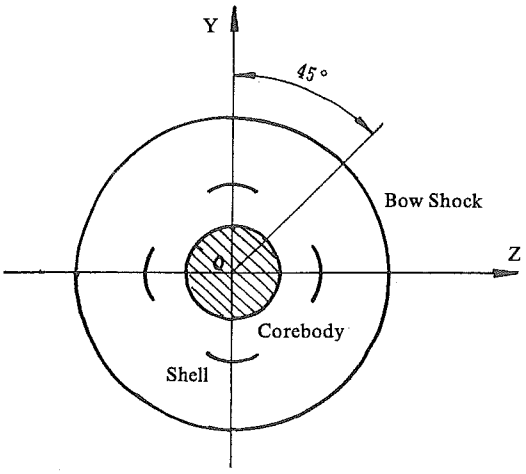

Figure 3 The 45° Fan Section in Space Marching Plane

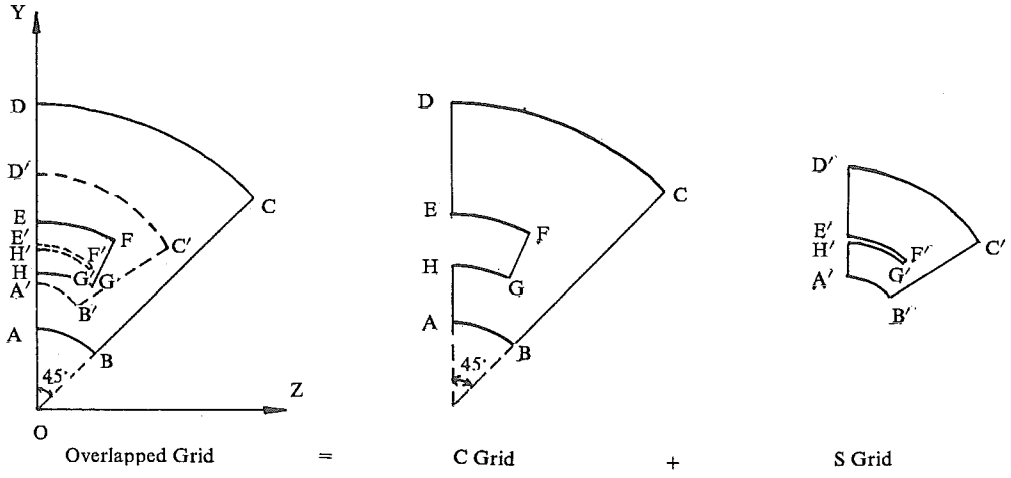

Figure 4 Structure of Overlapped Grid

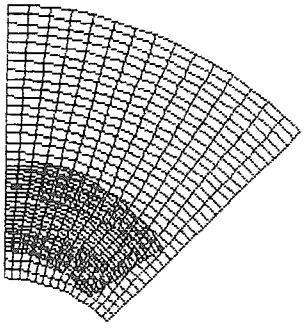

Figure 5-a The Overlapped Grid

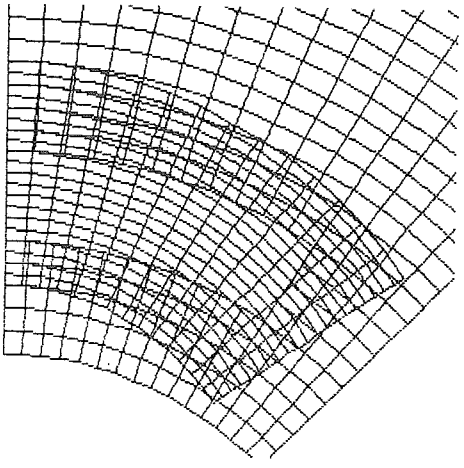

Figure 5-b Locally Enlargement of Overlapped Grid

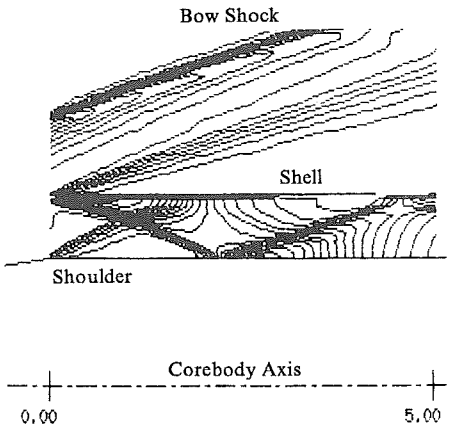

Figure 6 Iso-pressure Contour GAP = 0.82

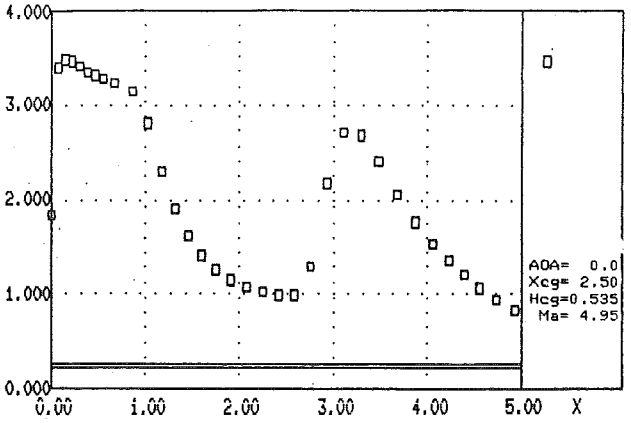

Figure 7 Pressure Distributon along the Lower Surface of Shell

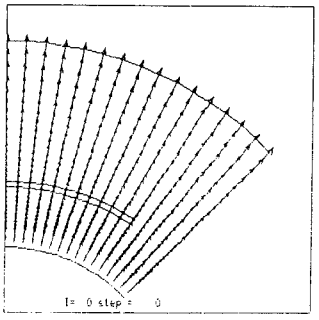

a. (X=0.0)

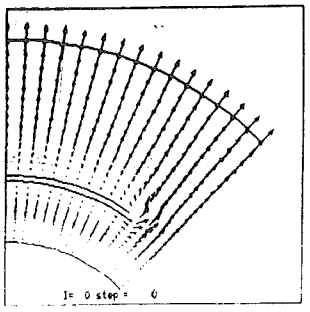

b. (X=0.96)

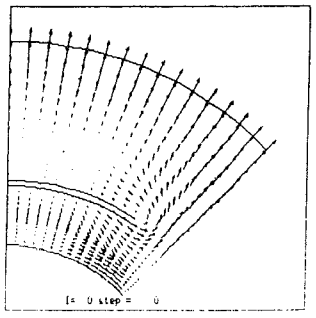

c. (X=2.3)

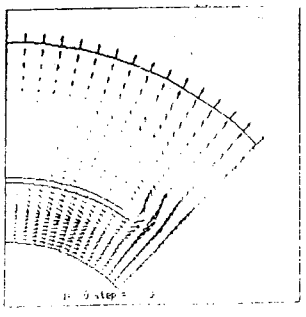

d. (X=4.2)

Figure 8 Velocity Vector in Different Space Marching Planes

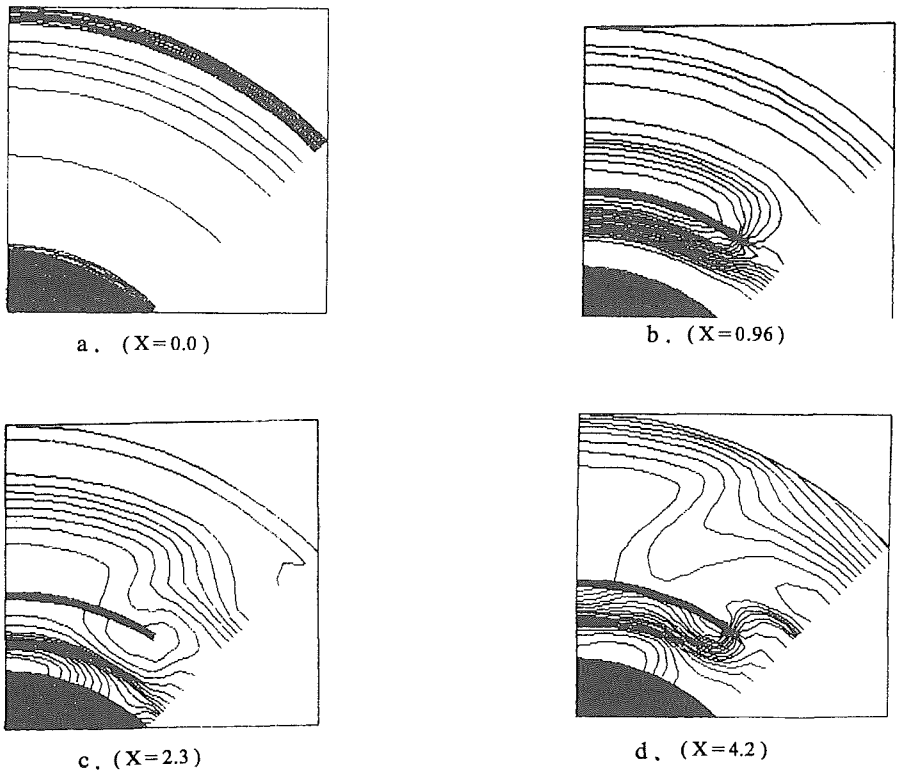

Figure 9 Iso-pressure Contours in Different Space Marching Planes

Table 1 Presure Centers of Shell at Different Positions and Attitudes

$\overline{X}_{cg}$	GAP	δ(deg)	$\overline{X}_{cp}$	$\overline{X}_{cg}$	GAP	δ(deg)	$\overline{X}_{cp}$
2.5005	0.267	0.000	−0.7865	2.5007	2.544	0.425	0.7913
2.5005	0.805	0.016	−1.3547	2.5011	3.184	0.574	1.5767
2.5005	1.357	0.089	−0.7394	2.5061	3.840	0.641	0.0801
2.5005	1.933	0.228	−0.3399	2.5019	4.170	0.665	−0.0226

where $\overline{X}_{cg}$ is meassured from corebody shoulder
$\overline{X}_{cp} < 0$ means pitching down .